J. Fluid Mech. (1991), *vol.* 226, *pp.* 425–443
Printed in Great Britain

On the temporal instability of a two-dimensional viscous liquid sheet

By XIANGUO LI† AND R. S. TANKIN
Mechanical Engineering Department, Northwestern University, Evanston, IL 60208, USA

(Received 13 February 1989 and in revised form 2 November 1990)

This paper reports a temporal instability analysis of a moving thin viscous liquid sheet in an inviscid gas medium. The results show that surface tension always opposes, while surrounding gas and relative velocity between the sheet and gas favour, the onset and development of instability. It is found that there exist two modes of instability for viscous liquid sheets – aerodynamic and viscosity-enhanced instability – in contrast to inviscid liquid sheets for which the only mode of instability is aerodynamic. It is also found that axisymmetrical disturbances control the instability process for small Weber numbers, while antisymmetrical disturbances dominate for large Weber numbers. For antisymmetrical disturbances, liquid viscosity, through the Ohnesorge number, enhances instability at small Weber numbers, while liquid viscosity reduces the growth rate and the dominant wavenumber at large Weber numbers. At the intermediate Weber-number range, liquid viscosity has complicated effects due to the interaction of viscosity-enhanced and aerodynamic instabilities. In this range, the growth rate curve exhibits two local maxima, one corresponding to aerodynamic instability, for which liquid viscosity has a negligible effect, and the other due to viscosity-enhanced instability, which is influenced by the presence and variation of liquid viscosity. For axisymmetrical disturbances, liquid viscosity always reduces the growth rate and the dominant wavenumber, aerodynamic instability always prevails, and although the regime of viscosity-enhanced instability is always present, its growth rate curve does not possess a local maximum.

1. Introduction

In most spray applications, liquid issues from an orifice in the form of either a circular jet (full cone) such as in diesel engines, or a thin liquid sheet such as produced by a swirl nozzle (hollow cone) in gas burners, or by a fan spray nozzle. The breakup mechanism of a circular liquid jet has been extensively investigated over the past century. A theoretical understanding of the breakup mechanism of low-speed circular jets has been well established (McCarthy & Molloy 1974; Bogy 1979), following Rayleigh's (1879) classical analysis of the capillary instability of a liquid cylinder. The dominant mode of instability leading to a jet breakup is axisymmetrical disturbances, which result in drop formation. A nonlinear analysis has been carried out by Yuen (1968) along with experimental investigations (Goedde & Yuen 1970). The effects of liquid viscosity and liquid velocity relative to the surrounding medium were introduced by Weber (1931) and Sterling & Sleicher (1975), respectively.

On the other hand, there has been little investigation of the breakup of a moving

† Present address: University of Waterloo, Ontario, Canada.

thin liquid sheet, which is also of importance in many of the practical applications mentioned above. The two plane interfaces between two fluids, one of which is a liquid (such as water or liquid hydrocarbon fuels) and the other a gas (such as air), are in dynamic equilibrium, though both fluids may be moving at different velocities. That is, neither kinetic nor interfacial tension forces are acting on the liquid. However, if a protuberance is produced on the interface owing to any disturbances, forces acting on the interfaces develop. The surface tension force always tends to restore the interface back into its original equilibrium position, while the disturbance-induced normal stresses in both liquid and gas generally enhance the degree of instability, i.e. increase the amplitude of the disturbance. A relative velocity between the liquid and gas promotes the growth of disturbances until the liquid sheet disintegrates into fragments, which rapidly contract into unstable ligaments under the effect of surface tension. Finally, the ligaments are broken into a multitude of droplets.

The characteristics of these instabilities have been analysed by Squire (1953) and Hagerty & Shea (1955) for inviscid liquid sheets of uniform thickness in an inviscid gas medium. Their results show that the dominant type of disturbance inducing instability and eventually leading to the breakup of the sheet into droplets is antisymmetrical, and surface tension effects always tend to smooth out any protuberances. The principal sources of sheet instability are the aerodynamic forces arising from the interaction of the sheet with the surrounding gas medium. The winner in the competition between the capillary forces and aerodynamic forces determines whether a disturbance will grow or decay. When the capillary forces dominate, disturbances will die out, and the sheet is stable; if the aerodynamic forces dominate, disturbances will be further enhanced. In the latter case, the sheet becomes unstable, at least according to linear stability theory. The ratio of the aerodynamic forces to the capillary forces is defined as the gas Weber number, We_g. Thus, when the gas Weber number exceeds a critical value, instability of the sheet occurs which in turn leads to the sheet breakup. This critical value was found by Squire (1953) to be $We_{gc} = \tilde{\rho} = \rho_g/\rho_\ell$ for antisymmetrical disturbances, where $\tilde{\rho}$ represents the gas to liquid density ratio. Dombrowski & Johns (1963) extended the analysis by including the effect of liquid viscosity. However, their results are only valid for large gas Weber numbers owing to approximations made in their analysis.

In summary, the breakup mechanisms for a low-speed circular liquid jet and for a moving thin liquid sheet have several distinctly different features (Reitz 1976; Lefebvre 1989):

(i) For the jet, the dominant type of disturbance which induces instability and eventually lead to its breakup into droplets is axisymmetrical; whereas it is antisymmetrical for the sheet.

(ii) For the jet, the principal sources of instability are the capillary forces for Rayleigh instability, and aerodynamics forces for wind-induced instability; while for the sheet they are the aerodynamic forces, i.e. due to the aerodynamic interaction of the sheet with its surrounding gas medium. Thus, without the presence of a gas medium (a vacuum environment), the sheet would always be stable.

(iii) For the jet, the effect of surface tension (or capillary force) induces instability (destabilizing) and results in drop formation at negligible relative velocity – Rayleigh instability; at finite relative velocity, surface tension reduces instability (stabilizing) – wind-induced instability. For the sheet, surface tension always opposes the onset and development of instability.

(iv) For the jet, the relative velocity between liquid and gas phases contributes

to, but is not necessary for breakup, whereas it is required for the breakup of the sheet.

In view of the above differences, a theoretical investigation has been conducted on the instability of a moving thin liquid sheet of uniform thickness, including the effect of liquid viscosity. Another motivation for the present work is that the moving thin liquid sheet is a reasonably good approximation to sheet breakup processes in hollow cone sprays, which has numerous practical applications.

The present study shows that at small gas Weber numbers, axisymmetrical disturbances control the instability processes, contrary to the conclusions reached by Squire (1953) and Hagerty & Shea (1955), while at slightly larger gas Weber numbers, antisymmetrical disturbances dominate. For antisymmetrical disturbances, the introduction of even small liquid viscosity changes the development of an instability drastically, especially at low Weber numbers. When the gas Weber number is smaller than a critical value, $We_{\mathrm{gc}} = \tilde{\rho}$, aerodynamic instability disappears and liquid viscosity under this condition enhances the disturbances. When the gas Weber number is larger than the critical Weber number, but still of comparable value; both viscosity-enhanced and aerodynamic instabilities interact with each other, displaying very complicated effects of liquid viscosity on the instability processes. When the gas Weber number substantially exceeds the critical value, aerodynamic instability dominates the instability processes, and liquid viscosity acts to reduce the growth rate and to shift the dominant disturbances to longer wavelengths. For axisymmetrical disturbances, liquid viscosity always reduces the growth rate and dominant wavenumber, aerodynamic instability always dominates, and the regime of viscosity-enhanced instability is always present, but in a much smaller range.

We are mainly interested in the phenomenon of the sheet breakup processes, which eventually lead to drop formation. Thus, the present study focuses primarily on the growth of the disturbance waves through an instability, and does not yield any prediction on the sizes of the subsequently formed drops. This latter point has been addressed theoretically by Li & Tankin (1987, 1988) through the application of the maximum entropy principle.

2. Dispersion relation for antisymmetrical disturbances

Consider a two-dimensional liquid sheet with density ρ_ℓ, viscosity μ_ℓ, surface tension σ and uniform thickness $2a$, moving at velocity U_0 through an inviscid stationary gas medium of density ρ_{g}. That is, the reference frame is attached to the surrounding gas medium; therefore the velocity U_0 can be regarded as the relative velocity of the liquid sheet and the gas medium. The velocity U_0 is small compared to the velocity of sound; thus the assumption of incompressibility for both fluids is valid. Gravitational effects are neglected. The coordinates are chosen such that the direction of the x-axis is parallel to the direction of the velocity U_0, and the y-axis is normal to the liquid sheet with its origin located at the midplane of the sheet. These quantities are illustrated in figure 1.

2.1. *Liquid–gas interfaces*

For antisymmetrical disturbances, the displacements of corresponding points on the two interfaces are equal in magnitude and in the same direction. Hence, the two interfaces are regarded to have the following form:

$$y = \pm a + \xi, \quad \xi = \xi_0 \exp(\omega t + \mathrm{i}kx), \tag{1}$$

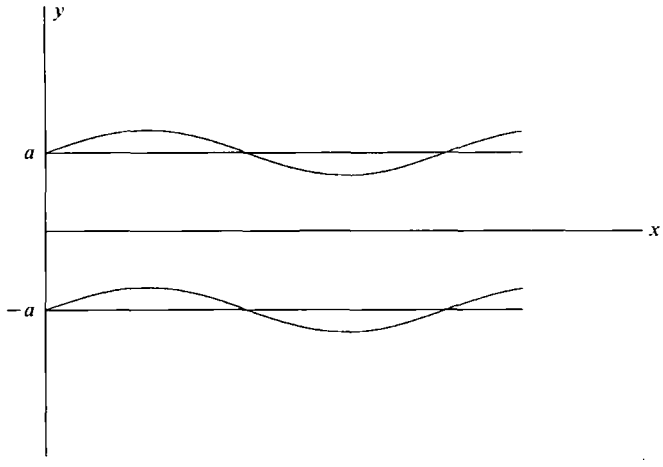

FIGURE 1. Antisymmetrical disturbances.

where $y = \pm a$ are the equilibrium positions of the two interfaces, i.e. the positions with no disturbances; ξ_0 is the initial amplitude of the disturbance, and is taken to be much smaller than the half-width of the sheet, a; k is the wavenumber of the disturbance, and $k = 2\pi/\lambda$, where λ is the wavelength of the disturbance; $\omega = \omega_r + i\omega_i$ is a complex variable. The real part of ω, ω_r, represents the rate of growth or decay of the disturbance; its imaginary part ω_i is 2π times the disturbance frequency; and $-\omega_i/k$ is the wave propagation velocity of the disturbance. Hence, the disturbance frequency and the wave velocity are related. t is the time and $i = \sqrt{-1}$.

2.2. *Liquid motion*

The base flow of the liquid sheet is a uniform flow of velocity U_0 along the x-direction, with zero velocity along the y-direction and ambient pressure (zero) in the liquid sheet. Assume u, v are the liquid velocity components in the x, y-directions, respectively, resulting from a disturbance, and p the pressure due to the disturbance. All these quantities (u, v and p) are presumed to be very small. The equations of continuity and motion are linearized by neglecting all nonlinear terms in these small disturbance quantities, and can be expressed as follows:

Continuity
$$\frac{\partial u}{\partial x} + \frac{\partial v}{\partial y} = 0; \tag{2}$$

Momentum
$$\frac{\partial u}{\partial t} + U_0 \frac{\partial u}{\partial x} = -\frac{1}{\rho_\ell}\frac{\partial p}{\partial x} + \nu_\ell \nabla^2 u, \tag{3}$$

$$\frac{\partial v}{\partial t} + U_0 \frac{\partial v}{\partial x} = -\frac{1}{\rho_\ell}\frac{\partial p}{\partial y} + \nu_\ell \nabla^2 v; \tag{4}$$

where
$$\nabla^2 = \frac{\partial^2}{\partial x^2} + \frac{\partial^2}{\partial y^2}$$

is the Laplacian operator, and ν_ℓ is the liquid kinematic viscosity.

Equations (2)–(4) are subjected to the following boundary conditions: at the two interfaces, which can be taken as $y \approx \pm a$ (first-order approximation in the small displacement of the interfaces, ξ, due to the disturbance), there should be no net mass flux across the interfaces. Thus, the normal velocity at the interfaces derived from

(2)–(4) should be equal to that derived from (1). The shear stress should vanish at the interfaces, and the normal stress across the interfaces should be continuous. These boundary conditions, in mathematical form, are

$$v = \frac{\partial \xi}{\partial t} + U_0 \frac{\partial \xi}{\partial x} \quad \text{at} \quad y \approx \pm a, \tag{5}$$

$$\tau_{xy} = \mu_\ell \left(\frac{\partial u}{\partial y} + \frac{\partial v}{\partial x} \right) = 0 \quad \text{at} \quad y \approx \pm a, \tag{6}$$

$$\tau_{yy} - \tau_{g,yy} = p_\sigma \quad \text{at} \quad y \approx \pm a, \tag{7}$$

where τ_{xy} and τ_{yy} are the liquid shear and normal stresses, and $\tau_{g,yy}$ is the gas normal stress. p_σ is the pressure induced by surface tension.

To solve (2)–(4), the liquid velocity is separated into two parts:

$$u = u_1 + u_2, \quad v = v_1 + v_2, \tag{8}$$

where (u_1, v_1) are the inviscid, irrotational solution in the liquid; thus, (u_2, v_2), which is left over, contains the effect of liquid viscosity.

As pointed out by Levich (1962), the pressure should be the same as that in an inviscid liquid because the presence of viscosity affects the wave frequency but not the pressure within the liquid. This approach was also adopted by Sterling & Sleicher (1975) in deriving the dispersion relation for the capillary instability of circular jets.

For inviscid liquid with irrotational flow, there exists a velocity potential, ϕ, such that

$$u_1 = \frac{\partial \phi}{\partial x}, \quad v_1 = \frac{\partial \phi}{\partial y}, \tag{9}$$

and ϕ satisfies

$$\nabla^2 \phi = 0. \tag{10}$$

The pressure is given by

$$p = -\rho_\ell \left(\frac{\partial \phi}{\partial t} + U_0 \frac{\partial \phi}{\partial x} \right). \tag{11}$$

Equations (2), (8)–(10) show that u_2 and v_2 are related as follows:

$$\frac{\partial u_2}{\partial x} + \frac{\partial v_2}{\partial y} = 0. \tag{12}$$

Equations (3) and (4) become, respectively,

$$\frac{\partial u_2}{\partial t} + U_0 \frac{\partial u_2}{\partial x} = \nu_\ell \nabla^2 u_2, \tag{13}$$

$$\frac{\partial v_2}{\partial t} + U_0 \frac{\partial v_2}{\partial x} = \nu_\ell \nabla^2 v_2. \tag{14}$$

Now let

$$u_2 = \frac{\partial \psi}{\partial y}, \quad v_2 = -\frac{\partial \psi}{\partial x}, \tag{15}$$

where ψ, very similar to a stream function, is an unknown function of the time and space coordinates. Equation (12) is automatically satisfied, and (13) and (14) reduce to

$$\frac{\partial \psi}{\partial t} + U_0 \frac{\partial \psi}{\partial x} = \nu_\ell \nabla^2 \psi. \tag{16}$$

Considering the disturbances given in (1), it is assumed that ϕ and ψ take the following form:

$$\phi = \Phi(y)\exp(\omega t + \mathrm{i}kx), \tag{17}$$

$$\psi = \Psi(y)\exp(\omega t + \mathrm{i}kx). \tag{18}$$

Substitution of (17) and (18) into (10) and (16) gives

$$\Phi''(y) - k^2\Phi(y) = 0, \tag{19}$$

$$\Psi''(y) - s^2\Psi(y) = 0, \tag{20}$$

where

$$s^2 = k^2 + \frac{\omega + \mathrm{i}kU_0}{\nu_\ell}.$$

Equations (19) and (20) can be easily solved to yield

$$\Phi(y) = C_1 \mathrm{e}^{ky} + C_2 \mathrm{e}^{-ky}, \tag{21}$$

$$\Psi(y) = C_3 \mathrm{e}^{sy} + C_4 \mathrm{e}^{-sy}, \tag{22}$$

where C_1, C_2, C_3, and C_4 are constants of integration to be determined later. Thus,

$$\phi = (C_1 e_{ky} + C_2 \mathrm{e}^{-ky})\exp(\omega t + \mathrm{i}kx), \tag{23}$$

$$\psi = (C_3 e_{sy} + C_4 \mathrm{e}^{-sy})\exp(\omega t + \mathrm{i}kx). \tag{24}$$

From the boundary conditions, (5) and (6), the unknown constants of integration are determined:

$$C_1 = -C_2 = \frac{k^2 + s^2}{2k\cosh(ka)}\nu_\ell \xi_0, \tag{25}$$

$$C_3 = C_4 = -\frac{\mathrm{i}k}{\cosh(sa)}\nu_\ell \xi_0, \tag{26}$$

whence the normal stress in the liquid sheet is

$$\tau_{yy} = -p + 2\mu_\ell \frac{\partial v}{\partial y}$$

$$= \{[\rho_\ell(\omega + \mathrm{i}kU_0) + 2\mu_\ell k^2](\mathrm{e}^{ky} - \mathrm{e}^{-ky})C_1 - \mathrm{i}2\mu_\ell ks(\mathrm{e}^{sy} - \mathrm{e}^{-sy})C_3\}\exp(\omega t + \mathrm{i}kx), \tag{27}$$

where C_1 and C_3 are given in (25) and (26).

2.3. *Gas motion*

In our present analysis, the effect of the surrounding gas medium on the instability of liquid sheet comes about through the normal stress in boundary condition (7). The gas medium is assumed to be inviscid, and stationary before the disturbances set in. Hence, the governing equations for the disturbed gas motion are:

Continuity

$$\frac{\partial u_g}{\partial x} + \frac{\partial v_g}{\partial y} = 0; \tag{28}$$

Momentum

$$\frac{\partial u_g}{\partial t} = -\frac{1}{\rho_g}\frac{\partial p_g}{\partial x}, \tag{29}$$

$$\frac{\partial v_g}{\partial t} = -\frac{1}{\rho_g}\frac{\partial p_g}{\partial y}; \tag{30}$$

where the subscript g denotes quantities for the gas medium. The boundary conditions for the inviscid gas require that across the liquid–gas interfaces the

normal velocity be continuous (tangential velocity could have a jump), and far away from the liquid sheet the effects of the disturbances die out. Hence the boundary conditions are

$$v_g = \frac{\partial \xi}{\partial t} \quad \text{at} \quad y \approx \pm a, \tag{31}$$

$$v_g = 0 \quad \text{as} \quad y \to \pm \infty. \tag{32}$$

Since the gas medium is regarded as inviscid, the velocity can be expressed in terms of a velocity potential. Furthermore, the velocity potential for the gas motion is assumed to be

$$\phi_g = \Phi_g(y) \exp(\omega t + ikx) \tag{33}$$

in accordance with the assumed form of the disturbance given in (1). Thus, (28) and the boundary conditions given in (31) and (32) yield

$$\phi_g = -(\omega/k) \exp[k(a-y)]\, \xi_0 \exp(\omega t + ikx) \quad \text{for} \quad y \geqslant a. \tag{34}$$

Hence, considering (29) and (30), the normal stress in the gas medium becomes

$$\tau_{g,yy} = -p_g = \rho_g \frac{\partial \phi_g}{\partial t}$$

$$= -\rho_g \frac{\omega^2}{k} \exp[k(a-y)]\, \xi_0 \exp(\omega t + ikx). \tag{35}$$

2.4. *Pressure induced by surface tension*

The pressure induced by surface tension is, to the first order in ξ,

$$p_\sigma = \frac{\sigma}{R} \approx \sigma \frac{\partial^2 \xi}{\partial x^2}$$

because ξ is taken to be very small. R is the radius of curvature of the interfaces. For antisymmetrical disturbances, ξ is given by (1). Hence, p_σ becomes

$$p_\sigma = -\sigma k^2 \xi_0 \exp(\omega t + ikx). \tag{36}$$

2.5. *Dispersion relation*

Substitution of (27), (35), and (36) into (7) for $y = a$ leads to the following dispersion relation between the complex growth rate ω and the disturbance wavenumber k:

$$[\rho_\ell(\omega + ikU_0) + 2\mu_\ell k^2][\nu_\ell(k^2+s^2)] \tanh(ka)$$
$$-4\mu_\ell \nu_\ell k^3 s \tanh(sa) + \rho_g \omega^2 + \sigma k^3 = 0, \tag{37}$$

where s depends on k, ω, U_0 and ν_ℓ.

3. Dispersion relation for axisymmetrical disturbances

The derivation process of the dispersion relation for axisymmetrical disturbances is very similar to that for antisymmetrical ones. The results are very similar to (37) except that $\tanh(ka)$ and $\tanh(sa)$ are now replaced by $\coth(ka)$ and $\coth(sa)$ respectively:

$$[\rho_\ell(\omega + ikU_0) + 2\mu_\ell k^2][\nu_\ell(k^2+s^2)] \coth(ka)$$
$$-4\mu_\ell \nu_\ell k^3 s \coth(sa) + \rho_g \omega^2 + \sigma k^3 = 0. \tag{38}$$

Equations (37) and (38) are very complicated, and analytical solutions for ω as a function of k do not exist; therefore a numerical solution is required. However, for certain limiting conditions, these equations can be solved analytically.

4. Analyses and discussion

The dispersion relations, (37) and (38), show clearly that the surface tension effects always tend to stabilize the liquid sheet; that is, to smooth out any protuberances on the sheet boundaries. However, for a circular liquid jet, surface tension may induce instability – Rayleigh's instability; or may reduce instability – wind-induced instability, depending on the relative velocity of the jet and ambient gas medium.

To facilitate the analysis, (37) and (38) are expressed non-dimensionally as follows:

$$(\tilde{\omega}_1+4m^2Z)\,\tilde{\omega}_1\tanh(m) + 4m^3Z^2[m\tanh(m)-(m^2+\tilde{\omega}_1/Z)^{\frac{1}{2}}\tanh(m^2+\tilde{\omega}_1/Z)^{\frac{1}{2}}]+\rho\tilde{\omega}^2+m^3=0, \quad (39)$$

$$(\tilde{\omega}_1+4m^2Z)\,\tilde{\omega}_1\coth(m) + 4m^3Z^2[m\coth(m)-(m^2+\tilde{\omega}_1/Z)^{\frac{1}{2}}\coth(m^2+\tilde{\omega}_1/Z)^{\frac{1}{2}}]+\rho\tilde{\omega}^2+m^3=0, \quad (40)$$

where $\tilde{\omega}=\tilde{\omega}_r+\mathrm{i}(We_\ell)^{\frac{1}{2}}\tilde{\omega}_i$, $\tilde{\omega}_1=\tilde{\omega}+\mathrm{i}(We_\ell)^{\frac{1}{2}}m$, $\tilde{\omega}_r=\omega_r/(\sigma/\rho_\ell a^3)^{\frac{1}{2}}$ and $\tilde{\omega}_i=\omega_i/(U_0/a)$. The other parameters in (39) and (40) are, respectively, the liquid Weber number, $We_\ell=\rho_\ell U_0^2 a/\sigma$, which represents the ratio of liquid inertial effects to capillary effects; and the Ohnesorge number, $Z=\mu_\ell/(\rho_\ell a\sigma)^{\frac{1}{2}}$, which is equal to the ratio of the square root of the liquid Weber number to the liquid Reynolds number. Hence Z is physically the ratio of viscous forces to capillary forces. $\tilde{\rho}$ denotes the density ratio of the surrounding gas to the liquid, and $m=ka$ is the dimensionless wavenumber.

For inviscid liquid, $\mu_\ell=0$ (that is, $Z=0$), (39) and (40) readily reduce to the results obtained by Squire (1953) and Hagerty & Shea (1955):

$$\tilde{\omega}_r=\frac{m}{\tilde{\rho}+\tanh(m)}\{We_g\tanh(m)-m[\tilde{\rho}+\tanh(m)]\}^{\frac{1}{2}} \quad (41)$$

for antisymmetrical disturbances; and

$$\tilde{\omega}_r=\frac{m}{\tilde{\rho}+\coth(m)}\{We_g\coth(m)-m[\tilde{\rho}+\coth(m)]\}^{\frac{1}{2}} \quad (42)$$

for axisymmetrical disturbances, where $We_g=\rho_g U_0^2 a/\sigma$ is the gas Weber number, which represents the ratio of aerodynamic forces (generated by the relative velocity between gas medium and liquid) exerted on perturbations on the liquid–gas interfaces, to capillary forces. It is clear from (41) and (42) that capillary forces (surface tension effects) always tend to stabilize the liquid sheet, that is, to damp out any disturbances; and aerodynamic forces are responsible for the occurrence of instability. In this sense, the instability expressed by (41) and (42) for an inviscid liquid sheet is termed *aerodynamic instability*.

It might be mentioned that the reference parameters chosen by Dombrowski & Johns (1963) for the non-dimensionalization of the growth rate and the disturbance wavenumber are not appropriate since the Weber number and the Ohnesorge number did not appear explicitly in the final form of their dispersion relation. These dimensionless numbers have been identified as key parameters in describing the jet breakup processes (Reitz 1976; Lefebvre 1989).

4.1. *Instability limits*

The instability limit is the maximum wavenumber of disturbances giving rise to instability, which corresponds to the positive value of the disturbance growth rate; that is, ω_r (or $\tilde{\omega}_r$) > 0. The wavenumber at the instability limit is usually called the limiting wave number, m_0, which can be obtained by setting ω_r (or $\tilde{\omega}_r$) $= 0$. For viscous liquid sheets, both (39) or (40) give the limiting wavenumber as

$$m_0 = We_g. \tag{43}$$

For inviscid liquid, the limiting wavenumber, $m_{0,I}$, can be obtained from (41) and (42), which become

$$We_g \tanh(m_{0,I}) - m_{0,I}[\tilde{\rho} + \tanh(m_{0,I})] = 0 \tag{44}$$

for antisymmetrical disturbances; and

$$We_g \coth(m_{0,I}) - m_{0,I}[\tilde{\rho} + \coth(m_{0,I})] = 0 \tag{45}$$

for axisymmetrical disturbances. It is interesting to note that the instability limit in the viscous case cannot be reduced to that appropriate in the inviscid case. This rather odd effect of viscosity on the instability will be explored later.

For long-wave disturbances, $m_{0,I} \ll 1$, $\tanh(m_{0,I}) \approx m_{0,I}$ and $\coth(m_{0,I}) \approx 1/m_{0,I}$, then (44) and (45) reduce to

$$m_{0,I} = We_g - \tilde{\rho} \tag{46}$$

for antisymmetrical disturbances; and

$$m_{0,I} = \frac{We_g}{1 + \tilde{\rho}(We_g)} \tag{47}$$

for axisymmetrical disturbances. From (46) it is clear that when the gas Weber number is less than its critical value, $We_{g,c} = \tilde{\rho}$, there will be no instability arising from the antisymmetrical disturbances. This result was first obtained by Squire (1953).

On the other hand, for short waves, $m_{0,I} \gg 1$, $\tanh(m_{0,I}) \approx 1$, and $\coth(m_{0,I}) \approx 1$, then both (44) and (45) reduce to

$$m_{0,I} = \frac{We_g}{1 + \tilde{\rho}}. \tag{48}$$

Generally, (44) and (45) have to be solved numerically. This has been done and one of the results is presented in figure 2 for the density ratio of $\tilde{\rho} = 0.1$. Curve 1 in the figure represents the limiting wavenumber for axisymmetrical disturbances on inviscid liquid sheets; curve 2 that for antisymmetrical disturbances on inviscid liquid sheets; and curve 3 that for viscous liquid sheets. It is clear from figure 2 and (46)–(48) that for non-viscous liquid sheets, the instability range for axisymmetrical disturbances is always wider than that for antisymmetrical disturbances; and both limiting wavenumbers approach the same asymptotic value of $We_g/(1+\tilde{\rho})$, from above for axisymmetrical disturbances and from below for antisymmetrical disturbances. The same instability range for each type of disturbance shown by Hagerty & Shea (1955) is due to the approximation they introduced.

Equation (43) indicates that liquid viscosity does not directly affect the range of hydrodynamic instability, which is shown to be governed by the ratio of aerodynamic

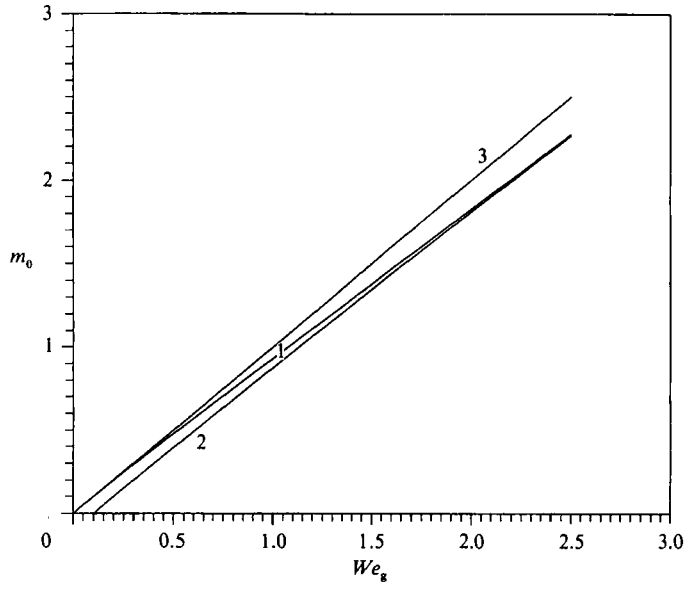

FIGURE 2. Limiting wavenumber for inviscid liquid sheets ($\tilde{\rho} = 0.1$; curve 1, axisymmetrical disturbances; curve 2, antisymmetrical disturbances) and viscous liquid sheets (curve 3).

forces to capillary forces. However, liquid viscosity does broaden the instability region. This can be seen by comparing (43) to either (44) or (45). It is even more evident if (43) is compared to the limiting cases presented in (46), (47), and (48). In figure 2, the region under curve 2 is the instability region for antisymmetrical disturbances due to aerodynamic interaction; that is, the region of aerodynamic instability mentioned before. The instability region between curves 2 and 3 is due to the presence of liquid viscosity. That is, there is a region of instability that is induced, or more precisely, enhanced by liquid viscosity. This mode of instability is henceforth termed *viscosity-enhanced instability*. For axisymmetrical disturbances, the region under curve 1 in figure 2 is the region of aerodynamic instability; while the region between curves 1 and 3 is viscosity-enhanced instability.

The finding of viscosity-enhanced instability might be very surprising at first, because the effect of viscosity, as might be expected, tends to damp out or dissipate disturbances under most situations. However, in the existing theory of hydrodynamic stability, there are at least three situations where the effect of fluid viscosity may have the opposite effect, depending on the flow conditions. The first description of the destabilizing effect of fluid viscosity on base flow field is due to Reynolds (1883). Although he was unable to suggest a physical mechanism by which viscosity would induce or enhance instability, he refused to exclude such a possibility. Heisenberg (1924) was the first to show mathematically that viscosity could actually cause instability in plane Poiseuille flow, which was later confirmed by Lin (1944). Another situation where viscosity may have destabilizing effect is the flow over a flat plate (that is, a Blasius boundary layer; for a discussion and more references, see Schlichting 1979). A third is the Bénard problem (thermal instability of a layer of fluid heated from below) under constant rotation (Chandrasekhar 1961).

As demonstrated by Tollmien (1929) for flow over a flat plate, the influence of viscosity on disturbances is significant not only in the immediate vicinity of the wall, but also in the neighbourhood of the critical layer, where the velocity of wave

propagation of the disturbances becomes equal to the velocity of the base flow. The presence of viscosity causes large changes in this critical layer. It is evident that viscosity plays a rather complicated dual role – on one hand it has a damping effect by dissipating energy; on the other, it is actually the cause of instability. At present, as pointed by Drazin & Reid (1981), the existing stability theory for viscous cases is not nearly as complete or general as for inviscid cases, and it provides only a partial understanding of the role of viscosity in those circumstances when it is the cause of instability.

For the present case of viscous liquid sheets having a constant base velocity, the inviscid part of the solution as given in (23) remains bounded at the critical layer, in contrast with unboundedness of its counterpart for flow over a flat plate. Also both the inviscid and viscous parts of the solution shown in (23) and (24) are valid up to the critical layer. However, liquid viscosity induces a shift in frequency of the disturbance; or equivalently, a change in the disturbance propagation velocity, as noted in the process of deriving the dispersion relation. Figure 3(*a*) demonstrates this change for viscous liquid sheets, where the two dashed curves represent the two stable waves of antisymmetrical disturbances on an inviscid liquid sheet, one propagating downstream, and the other upstream. It is clear that for aerodynamic instability (corresponding to a wavenumber between 0 and $m_{0,\mathrm{I}} = 0.06$), liquid viscosity has little effect. As seen in the figure, the results for inviscid and viscous liquid sheets coincide. However, over the wavenumber range from $m_{0,\mathrm{I}} = 0.06$ to $m_0 = 0.16$, the inviscid liquid sheet is stable (shown as dashed curves in the figure), while the presence of liquid viscosity shifts the wave velocity to a higher value, and the disturbance becomes unstable, which is labelled as viscosity-enhanced instability in figure 3(*a*). Over this range, the solid curve in this figure actually represents the results for $Z = 0.1$, 5, and 10, indicating that the disturbance frequency is changed only by the presence of liquid viscosity, but not its numerical value.

Apart from the frequency shift, liquid viscosity also results in a phase shift in the liquid and gas pressure fluctuations. The gas and liquid pressures at the interfaces for antisymmetrical disturbances are

$$p_{\mathrm{g}} \frac{a}{\sigma} = \rho\omega^2 \frac{1}{m}\left(\frac{\xi}{a}\right), \tag{49}$$

$$P \frac{a}{\sigma} = (\tilde{\omega}_1^2 + 2Zm^2\tilde{\omega}_1)\tanh(m)\frac{1}{m}\left(\frac{\xi}{a}\right), \tag{50}$$

where ξ is given in (1). For the axisymmetrical disturbances, $\tanh(m)$ in (50) is replaced by $\coth(m)$.

The phase difference between the liquid and gas pressures at the interface is calculated from (49) and (50). One typical result is shown in figure 3(*b*) where the parameters are the same as those in figure 3(*a*). In the wavenumber range of $m_{0,\mathrm{I}} = 0.06 \leqslant m \leqslant m_0 = 0.16$, the phase difference for inviscid liquid sheets (dashed, $Z = 0$) is 180°, indicating that the liquid and gas pressures oscillate exactly out of phase. However, for the viscous liquid sheets, the gas and liquid pressure fluctuations are in phase – at least for part of each cycle (see figure 3*b*). This in-phase pressure fluctuation resonates with the aerodynamic waves on the interfaces, leading to amplification of disturbances. The resonant effect of pressure fluctuations has also been suggested by Lin & Kang (1987) as the primary mechanism for the atomization of circular liquid jets. The physical importance of the phase shift near the critical

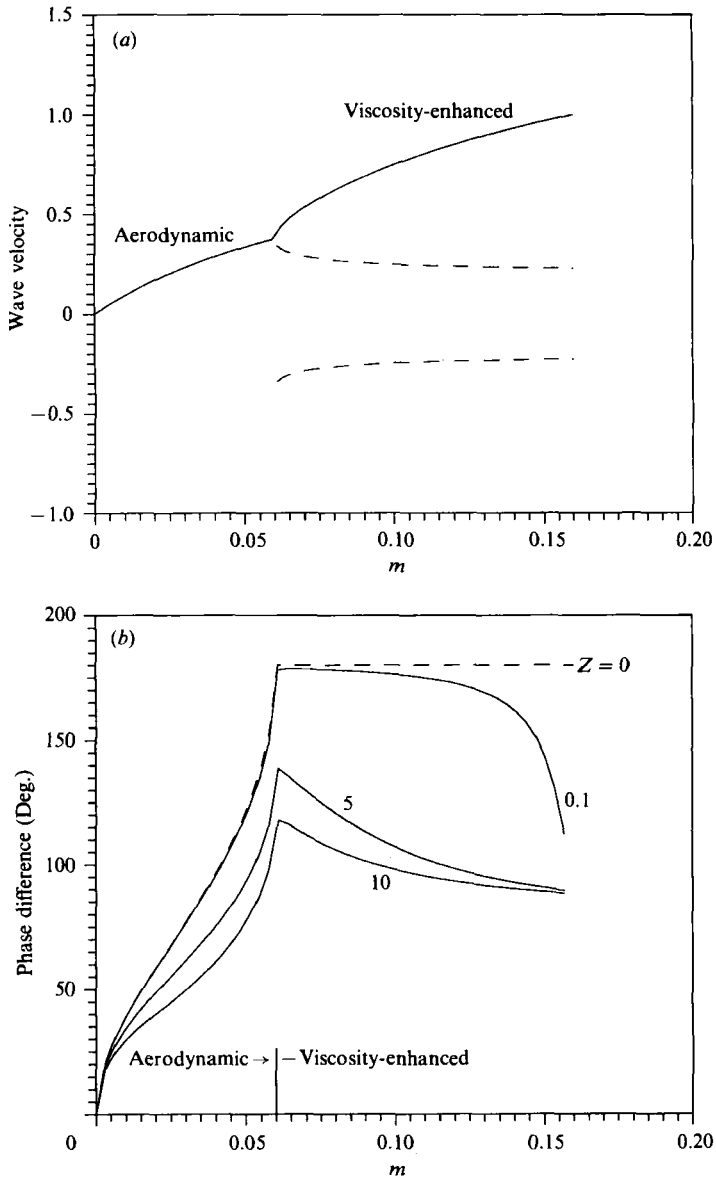

FIGURE 3. (*a*) Wave velocity normalized by base flow velocity for antisymmetrical disturbances; $\tilde{\rho} = 0.1$ and $We_g = 0.16$. (*b*) Phase difference between liquid and gas pressure fluctuations at the interfaces for antisymmetrical disturbances; $\tilde{\rho} = 0.1$ and $We_g = 0.16$.

layer due to viscosity as an instability mechanism was first pointed out by Prandtl (1921) and illustrated by Tollmien's (1929) calculation.

Recently Frankel & Weihs (1987) demonstrated that, for a stretching jet, the destabilizing effect of viscosity is produced by an axial viscous force. However, it can be shown that such a mechanism for instability is directly associated with the stretching of the jet, i.e. the axial velocity gradient in the base flow. For a non-stretching jet (constant base flow velocity) as studied by Sterling & Sleicher (1975), the axial viscous force does not exist. Similarly, it can also be shown that for the

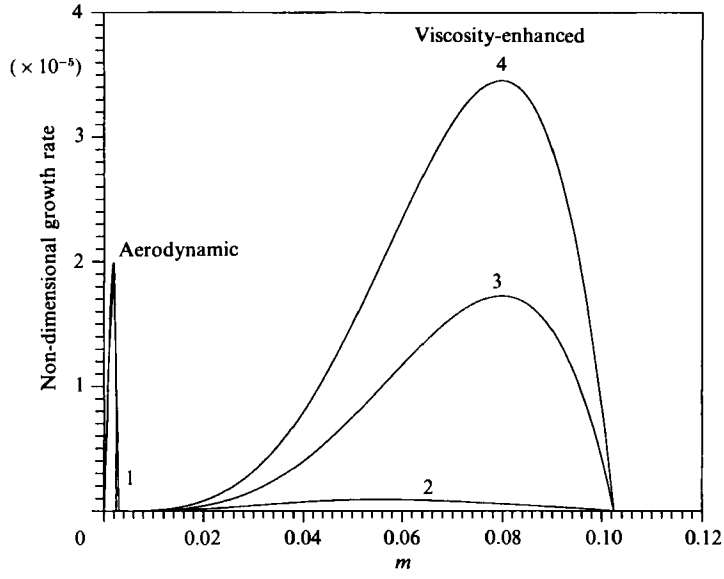

FIGURE 4. Non-dimensional growth rate for antisymmetrical disturbances. $\tilde{\rho} = 0.1$ and $We_g = 0.1025$. Curve 1, $Z = 0$; curve 2, $Z = 0.1$; curve 3, $Z = 5$; curve 4, $Z = 10$.

present case of a liquid sheet with constant base flow velocity such a mechanism for the destabilizing effect of viscosity cannot be present.

4.2. *Disturbance growth rate*

The growth rate is obtained by solving (39) or (40) through Muller's method. Figure 4 shows the non-dimensional growth $\tilde{\omega}_r$ for antisymmetrical disturbances. The density ratio is $\tilde{\rho} = 0.1$ and gas Weber number is $We_g = 0.1025$, which is just slightly larger than the critical value $We_{g,c} = \tilde{\rho} = 0.1$. Curve 1 in the figure corresponds to an inviscid liquid sheet ($Z = 0$), and thus represents aerodynamic instability; curve 2 is for a viscous liquid sheet of $Z = 0.1$; curve 3 is for $Z = 5$ and curve 4 for $Z = 10$. It is evident that for this case liquid viscosity, through Ohnesorge number Z, has little effect on aerodynamic instability, while it increases the growth rate dramatically for the mode of viscosity-enhanced instability, which dominates instability process under the condition of $Z = 10$. When We_g is smaller than $We_{g,c} = \tilde{\rho}$, then the aerodynamic instability disappears completely; only viscosity-enhanced instability will exist, and its growth rate curves are very similar to those shown in figure 4. Notice, particularly, the existence of two local maxima for viscous liquid sheets in this case. It should be pointed out that for curves 2, 3, and 4 in the figure, there is a range of wavenumbers ($m \approx 0.003$–0.014) for which the growth rate is very small ($\tilde{\omega}_r \approx O(10^{-9})$), but still positive. Hence it represents an unstable wave.

However, when the gas Weber number becomes very large in comparison with $We_{g,c}$, as is the case shown in figure 5, there is no local maximum growth rate for viscosity-enhanced instability – aerodynamic instability controls the sheet instability process. Liquid viscosity, effected through Ohnesorge number, reduces both the disturbance growth rate and shifts the dominant wave of the disturbances to a longer wavelength.

For axisymmetrical disturbances, the growth rate curves are always similar whether the gas Weber number is small or large. Aerodynamic instability always

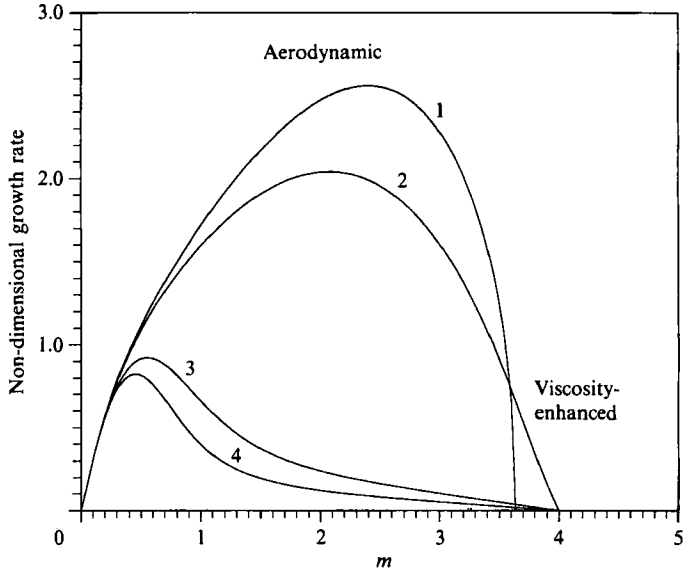

FIGURE 5. Non-dimensional growth rate for antisymmetrical disturbances. $\tilde{\rho} = 0.1$ and $We_g = 4$. Curve 1, $Z = 0$; curve 2, $Z = 0.1$; curve 3, $Z = 5$; curve 4, $Z = 10$.

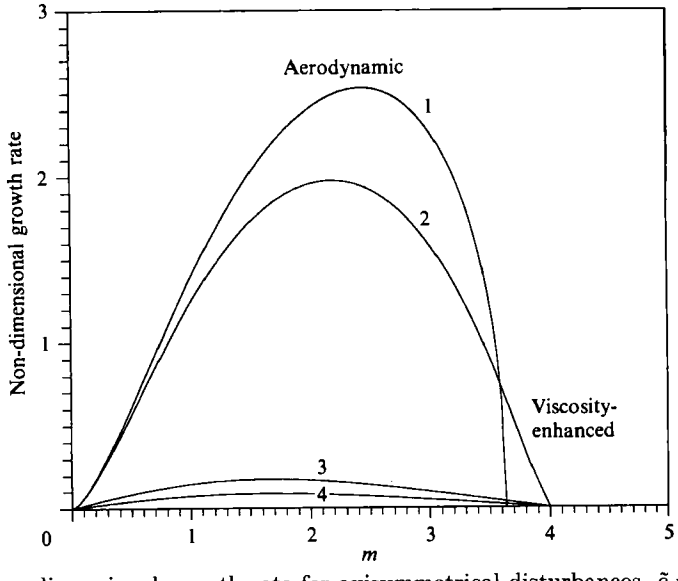

FIGURE 6. Non-dimensional growth rate for axisymmetrical disturbances. $\tilde{\rho} = 0.1$ and $We_g = 4$. Curve 1, $Z = 0$; curve 2, $Z = 0.1$; curve 3, $Z = 5$; curve 4, $Z = 10$.

prevails, and viscosity-enhanced instability has no local maximum growth rate. Liquid viscosity inhibits the development of disturbances, and reduces the growth rate quite effectively. Typical results are shown in figure 6.

4.3. *Maximum growth rate and dominant wavenumber*

The maximum growth rate and dominant wavenumber can be obtained from the condition $d\tilde{\omega}_r/dm = 0$ and the dispersion relations. Figures 7 and 8 show these quantities for the aerodynamic instability of an inviscid liquid sheet. The solid lines

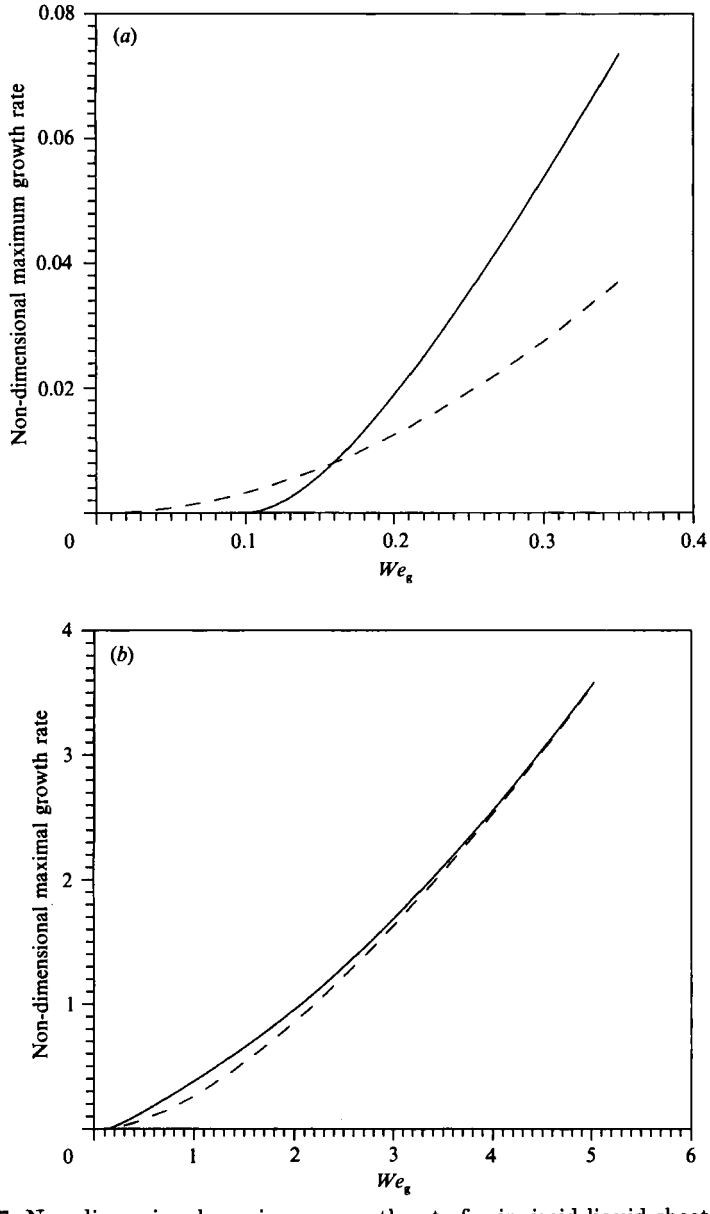

FIGURE 7. Non-dimensional maximum growth rate for inviscid liquid sheets. $\tilde{\rho} = 0.1$. Solid curve, antisymmetrical disturbances; dashed curve, axisymmetrical disturbances.

correspond to antisymmetrical disturbances, and the dashed curves to axisymmetrical disturbances. Figure 7(*a*) indicates that at small gas Weber number, axisymmetrical disturbances have a larger growth rate than antisymmetrical ones; they dominate the instability process. As the gas Weber number increases, the maximum growth rate for both types of disturbances increases. However, that of antisymmetrical disturbances increases much faster and, above a certain gas Weber number, antisymmetrical disturbances become predominant (figure 7*a*), and maintain this dominance over a wide range of gas Weber numbers (figure 7*b*). This is especially true at lower values of density ratios. This is the range of practical

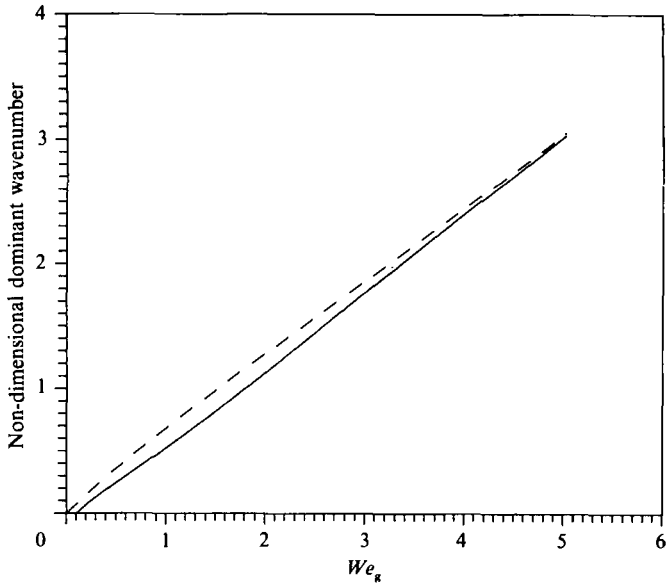

FIGURE 8. Non-dimensional dominant wavenumber for inviscid liquid sheets. $\tilde{\rho} = 0.1$. Solid curve, antisymmetrical disturbances; dashed curve, axisymmetrical disturbances.

interest, which both Squire (1953) and Hagerty & Shea (1955) have studied. That is why they had concluded that antisymmetrical disturbances are more detrimental for inviscid liquid sheets. However, at very large gas Weber numbers, it is seen in figure 7(*b*) that the maximum growth rates for both types of disturbances approach each other, indicating that they become equally important. But this regime is rarely reached in practice, for the density ratio of gas to liquid encountered in practice is much smaller than the value of 0.1 used here.

Figure 8 shows that for given conditions (fixed $\tilde{\rho}$ and We_g) the dominant wavenumber for axisymmetrical disturbances is always larger than the corresponding value for antisymmetrical ones, except for very large gas Weber numbers where both types of disturbances reach asymptotically the same dominant wavenumber. The latter is consistent with the results of maximum growth rates shown in figure 7(*b*).

Note that in figures 7 and 8, the maximum growth rate and dominant wavenumber for $We_g \leqslant We_{g,c} = \tilde{\rho}$ vanish for antisymmetrical disturbances. As discussed in §4.1, the instability does not exist for antisymmetrical disturbances under such conditions.

For antisymmetrical disturbances, the effect of liquid viscosity via the Ohnesorge number is very complicated (see table 1). As noted in the previous section, there exist two local maxima of the growth rate at small Weber numbers, due to the presence of the two different modes of instability. However, the local maximum for aerodynamic instability disappears as the gas Weber number becomes smaller than its critical value, while the local maximum for viscosity-enhanced instability vanishes at higher gas Weber numbers. The maximum growth rate is substantially increased by an increase in Z for viscosity-enhanced instability; whereas it is hardly changed for aerodynamic instability at small gas Weber numbers. Although there is evidence, seen in table 1, that liquid viscosity slightly increases the maximum growth rate for $We_g = 0.1025$ and 0.11, at $We_g = 0.16$ and 0.2 initially liquid viscosity increases the maximum growth rate (see $Z = 0.1$ and 5), and then reduces it (see

	Antisymmetrical disturbances							Axisymmetrical disturbances			
	Viscosity-enhanced			Aerodynamic				Aerodynamic			
We_g	$Z = 0.1$	$Z = 5$	$Z = 10$	$Z = 0$	$Z = 0.1$	$Z = 5$	$Z = 10$	$Z = 0$	$Z = 0.1$	$Z = 5$	$Z = 10$
0.05	0.12146×10^{-7}	0.43480×10^{-6}	0.86954×10^{-6}	0	—	—	—	0.80419×10^{-3}	0.59033×10^{-3}	0.31171×10^{-4}	0.15615×10^{-4}
0.1	0.77021×10^{-6}	0.15198×10^{-4}	0.30390×10^{-4}	0	—	—	—	0.31852×10^{-2}	0.23430×10^{-2}	0.12430×10^{-3}	0.62459×10^{-4}
0.1025	0.90593×10^{-6}	0.17281×10^{-4}	0.34554×10^{-4}	0.19923×10^{-4}	0.19930×10^{-4}	0.19930×10^{-4}	0.19930×10^{-4}	0.33448×10^{-2}	0.24607×10^{-2}	0.13099×10^{-3}	0.65621×10^{-4}
0.11	0.14548×10^{-5}	0.24978×10^{-4}	0.49943×10^{-4}	0.30212×10^{-3}	0.30255×10^{-3}	0.30255×10^{-3}	0.30255×10^{-3}	0.38464×10^{-2}	0.28306×10^{-2}	0.15086×10^{-3}	0.75575×10^{-4}
0.16	—	0.18438×10^{-3}	0.36845×10^{-3}	0.81191×10^{-2}	0.81715×10^{-2}	0.81751×10^{-2}	0.81719×10^{-2}	0.80554×10^{-2}	0.59412×10^{-2}	0.31915×10^{-3}	0.15989×10^{-3}
0.2	—	—	—	0.18834×10^{-1}	0.18983×10^{-1}	0.19002×10^{-1}	0.18973×10^{-1}	0.12482×10^{-1}	0.92232×10^{-2}	0.49864×10^{-3}	0.24983×10^{-3}
0.5	—	—	—	0.13806	0.13679	0.13255	0.12808	0.73062×10^{-1}	0.54787×10^{-1}	0.31151×10^{-2}	0.15612×10^{-2}
1.0	—	—	—	0.37901	0.36063	0.30416	0.28186	0.26118	0.20039	0.12436×10^{-1}	0.62358×10^{-2}
2.0	—	—	—	0.95485	0.84243	0.55626	0.50308	0.85247	0.67014	0.48865×10^{-1}	0.24535×10^{-1}
3.0	—	—	—	1.6821	1.3970	0.75331	0.67548	1.6264	1.2798	0.10488	0.52743×10^{-1}
4.0	—	—	—	2.5578	2.0399	0.92248	0.82320	2.5324	1.9730	0.17380	0.87534×10^{-1}
5.0	—	—	—	3.5618	2.7635	1.0741	0.95530	3.5512	2.7285	0.25048	0.12633

TABLE 1. Maximum growth rate for $\tilde{\rho} = 0.1$

	Antisymmetrical disturbances							Axisymmetrical disturbances			
	Viscosity-enhanced			Aerodynamic				Aerodynamic			
We_g	$Z = 0.1$	$Z = 5$	$Z = 10$	$Z = 0$	$Z = 0.1$	$Z = 5$	$Z = 10$	$Z = 0$	$Z = 0.1$	$Z = 5$	$Z = 10$
0.05	0.33650×10^{-1}	0.39886×10^{-1}	0.39887×10^{-1}	0	—	—	—	0.37300×10^{-1}	0.33858×10^{-1}	0.25062×10^{-1}	0.25016×10^{-1}
0.1	0.54893×10^{-1}	0.78008×10^{-1}	0.78015×10^{-1}	0	—	—	—	0.74198×10^{-1}	0.67428×10^{-1}	0.50124×10^{-1}	0.50031×10^{-1}
0.1025	0.55717×10^{-1}	0.79845×10^{-1}	0.79852×10^{-1}	0.18691×10^{-2}	0.18694×10^{-2}	0.18697×10^{-2}	0.18696×10^{-2}	0.76032×10^{-1}	0.69099×10^{-1}	0.51377×10^{-1}	0.51282×10^{-1}
0.11	0.57937×10^{-1}	0.85301×10^{-1}	0.85310×10^{-1}	0.74084×10^{-2}	0.74175×10^{-2}	0.74176×10^{-2}	0.74176×10^{-2}	0.81529×10^{-1}	0.74108×10^{-1}	0.55136×10^{-1}	0.55034×10^{-1}
0.16	—	0.11834	0.11836	0.42303×10^{-1}	0.42566×10^{-1}	0.42584×10^{-1}	0.42566×10^{-1}	0.11794	0.10733	0.80198×10^{-1}	0.80050×10^{-1}
0.2	—	—	—	0.68424×10^{-1}	0.68988×10^{-1}	0.69047×10^{-1}	0.68918×10^{-1}	0.14679	0.13371	0.10025	0.10006
0.5	—	—	—	0.24377	0.24198	0.22747	0.21542	0.35544	0.32600	0.25058	0.25012
1.0	—	—	—	0.52040	0.49150	0.35594	0.31414	0.67883	0.62773	0.49997	0.49904
2.0	—	—	—	1.1247	0.98708	0.45904	0.38793	1.2780	1.1820	0.97183	0.96986
3.0	—	—	—	1.7674	1.5266	0.51404	0.42643	1.8600	1.6960	1.3596	1.3560
4.0	—	—	—	2.4000	2.0760	0.55307	0.45322	2.4462	2.1915	1.6534	1.6472
5.0	—	—	—	3.0197	2.6118	0.58414	0.47413	3.0404	2.6814	1.8775	1.8679

TABLE 2. Dominant wavenumber for $\tilde{\rho} = 0.1$

$Z = 10$). At large gas Weber numbers, the maximum growth rate is reduced drastically.

For axisymmetrical disturbances, there is no local maximum of the growth rate for viscosity-enhanced instability. Liquid viscosity always decreases the maximum growth rate for aerodynamic instability (which always prevails for this type of disturbance). It is clear from table 1, for an axisymmetrical disturbance, that liquid viscosity is effective in reducing the maximum growth rate. For all modes of instability, table 1 shows that the maximum growth rate increases with gas Weber number, and also confirms that the general results for inviscid liqud sheets are also valid for viscous liquid sheets. That is, at small gas Weber numbers axisymmetrical disturbances are more dangerous to sheet stability; while at high gas Weber numbers antisymmetrical disturbances are more detrimental to sheet stability. In the intermediate range, the growth rate for both types of disturbances becomes comparable, signifying their equal importance in the development of instability processes. However, the dominant wavenumbers are different for each type of disturbance, for example see $We_g = 0.16$ and $Z = 0$–0.1 in tables 1 and 2 or figures 7 and 8. This may indicate the origin of the bimodal distribution of the subsequently formed drop sizes; if it is assumed, as is usual, that the size of the drops is proportional to the wavelength of dominant disturbances.

Table 2 shows the dominant wavenumber, corresponding to the maximum growth rate given in table 1. The general tendency of the variations of the dominant wavenumber and the effects of liquid viscosity resemble closely those of the maximum growth rate – except that liquid viscosity is more effective in reducing the dominant wavenumber of antisymmetrical disturbances.

For most practical applications, aerodynamic instability of antisymmetrical disturbances prevails (that is, $We_g \gg We_{g,c} = \tilde{\rho}$), since the density ratio and Ohnesorge number are usually very small. For example, a water sheet in atmospheric air gives $\tilde{\rho} = O(10^{-3})$ and $Z = O(10^{-2})$ for sheets as thin as 10 μm, and $Z = O(10^{-1})$ for sheet thickness of 1 μm; and the disturbances are still waves of long wavelength, such that $\tanh(m) \approx m$ is valid. Furthermore, for the dominance of aerodynamic instability, $\tilde{\rho}/m \ll 1$ holds. The above approximations have been considered by Squire (1953), Hagerty & Shea (1955) as well as many other investigators of this subject. Under these conditions, the maximum growth rate $\tilde{\omega}_r^*$ and dominant wavenumber m^* can be obtained from (39) by perturbation expansion techniques in terms of the small parameter Z; that is,

$$\tilde{\omega}_r^* = \tilde{\omega}_{r,I}^* - 2\tilde{\omega}_{r,I}^* Z, \tag{51}$$

and

$$m^* = m_I^* - 2m_I^{*2} Z, \tag{52}$$

where $m_I^* = \frac{1}{2}We_g$ and $\tilde{\omega}_{r,I}^* = \frac{1}{2}We_g$ are the dominant wavenumber and maximum growth rate, respectively, for inviscid liquid sheets, a result obtained originally by Squire (1953). It is clear that for the prevailing aerodynamic instability (of antisymmetrical disturbances) on a liquid sheet in a gas medium, liquid viscosity acts to reduce the dominant wavenumber and shift the dominant disturbance to a longer wavelength.

5. Conclusions

This paper reports a temporal instability analysis of a moving thin viscous liquid sheet in an inviscid gas medium. The results show that surface tension always opposes, while surrounding gas and relative velocity between the sheet and gas

favour, the onset and development of instability. It is found that there exist two modes of instability for viscous liquid sheets – aerodynamic and viscosity-enhanced instability – in contrast to inviscid liquid sheets for which the only mode of instability is aerodynamic. It is also found that axisymmetrical disturbances control the instability process for small Weber numbers; while antisymmetrical disturbances dominate for large Weber numbers.

For antisymmetrical disturbances, liquid viscosity, through Ohnesorge number, enhances instability at small Weber numbers, while reducing the growth rate and dominant wavenumber at large Weber numbers. At an intermediate Weber-number range, liquid viscosity has complicated effects due to the interaction of viscosity-enhanced and aerodynamic instabilities. In this range, the growth rate curve exhibits two local maxima, one corresponding to aerodynamic instability, for which liquid viscosity has vanishing effect, and the other due to viscosity-enhanced instability, which is greatly influenced by the presence and variation of liquid viscosity.

For axisymmetrical disturbances, liquid viscosity always reduces the growth rate and dominant wavenumber, and aerodynamic instability always prevails. The regime of viscosity-enhanced instability is always present, but its growth rate curve does not possess a local maximum.

At large Weber numbers, liquid viscosity is more effective in reducing the growth rate of axisymmetrical disturbances than antisymmetrical disturbances. Liquid viscosity is more effective in decreasing the dominant wavenumber of antisymmetrical disturbances than that of axisymmetrical disturbances.

REFERENCES

Bogy, D. B. 1979 *Ann. Rev. Fluid Mech.* **11**, 207.

Chandrasekhar, C. 1961 *Hydrodynamic and Hydromagnetic Stability.* Oxford University Press.

Dombrowski, N. & Johns, W. R. 1963 *Trans. ASME* E: *Chem. Engng Sci.* **18**, 203.

Drazin, P. G. & Reid, W. H. 1981 *Hydrodynamic Stability.* Cambridge University Press.

Franke, I. & Weihs, D. 1987 *J. Fluid Mech.* **185**, 361.

Goeddé, E. F. & Yuen, M. C. 1970 *J. Fluid Mech.* **40**, 495.

Hagerty, W. W. & Shea, J. F. 1955 *J. Appl. Mech.* **22**, 509.

Heisenberg, W. 1924 *Ann. Phys.* **74**, 577.

Lefebvre, A. H. 1989 *Atomization and Sprays.* Hemisphere.

Levich, V. G. 1962 *Physicochemical Hydrodynamics.* Prentice-Hall.

Li, X. & Tankin, R. S. 1987 *Combust. Sci. Tech.* **56**, 65.

Li, X. & Tankin, R. S. 1988 *Combust. Sci. Tech.* **60**, 345.

Lin, C. C. 1944 *Proc. Natl Acad. Sci. USA* **30**, 316.

Lin, S. P. & Kang, D. J. 1987 *Phys. Fluids* **30**, 2000.

McCarthy, M. J. & Molloy, N. A. 1974 *Chem. Engng J.* **7**, 1.

Prandtl, L. 1921 *Z. Angew. Math. Mech.* **1**, 431.

Rayleigh, Lord 1879 *Proc. Lond. Math. Soc.* **X**, 4.

Reitz, R. D. 1976 *AMS Rep.* 1262.

Reynolds, O. 1883 *Phil. Trans. R. Soc. Lond.* **174**, 935.

Schlichting, H. 1979 *Boundary-Layer Theory.* McGraw-Hill.

Squire, H. B. 1953 *Brit. J. Appl. Phys.* **4**, 167.

Sterling, A. M. & Sleicher, C. A. 1975 *J. Fluid Mech.* **68**, 477.

Tollmien, W. 1929 *Math. Phys.* Kl., pp. 21–44. (Also Engl. transl. in *NACA TM* 609, 1931).

Weber, K. 1931 *Z. Angew Math. Mech.* **11**, 136.

Yuen, M. C. 1968 *J. Fluid Mech.* **33**, 151.